Active Damping Actuators Combined with Passive Guidance Force of Polarized Linear Motor - Application to Swissmetro

No. 20

[1)]A. Cassat, [2)]C. Espanet, [3)]V. Bourquin, [4)]Y. Perriard

[1), 4)]Ecole Polytechnique Fédérale de Lausanne, EPFL-STI-IPR-LAI, CH-1015 Lausanne, Suisse
Phone: +41(0)21 693 26 91 – Fax: +41(0)21 693 26 87 – e-mail: alain.cassat@epfl.ch
[2)]University of Franche-Comté, France, Laboratory of Research in Electrical Engineering and Systems
Phone: +33(0)3 845 8 3614 – Fax: +33(0)3 845 8 3636 – e-mail: christophe.espanet@univ-fcomte.fr
[3)]Numexia Capital SA, CH-1040 Echallens, Suisse
Phone: +41(0)21 886 1515 – e-mail: vincent.bourquin@numexia.com

ABSTRACT: High speed Maglev (>400 km/h) refer to high speed levitated systems such as the Japanese JR-Maglev MLX and the German Transrapid. The Swissmetro Project, presenting a unique aspect of Maglev, is designed to work under partial vacuum (<10 kPa) in two tunnels.

In previous papers, the authors investigated the combination of the propulsion with the levitation. To minimize the heat due to the iron and copper losses, a polarized excitation is proposed with NdFeB PM for the magnetic way poles. Related to this function combination, the authors studied the passive guidance forces (reluctance effect), produced by the magnetic way. As it was proven that the passive damping produced by the magnetic way iron losses are not enough to damp the oscillations, when the real track profile creates pulsations closed to the eigen pulsation, additional damping actuators are necessary.

This paper emphases the design of these additional damping actuators. The dynamics of the passive guidance forces, combined with the damping forces of the additional actuators and the interaction of the real profile of the long stator track, is fully determined. Finite element 3D simulations of the magnetic system and Simulink simulations of the mechanical system and the control permit to confirm the proposed solution of the vehicle guidance.

KEYWORDS: PASSIVE FORCE, GUIDANCE, LINEAR MOTORS, MAGLEV, PERMANENT MAGNET, SWISSMETRO

1 INTRODUCTION

For high speed Maglev[(1)](>400 km/h), only linear synchronous motors are considered for the propulsion. For the Swissmetro Project[(2)], a new combination of the propulsion with the levitation, is considered involving, for the motor excitation, permanent magnets of high energy combined with windings (for the levitation control). For the vehicle lateral guidance, References[(3,4,5,6)] present the determination of the static guidance forces, produced by the magnetic way, and a first order analysis of the corresponding lateral dynamic behavior. The presented results emphasis that the passive damping produced by the *iron losses* of the magnetic way is not enough to damp the oscillations, when the track profile creates mechanical pulsations closed to the eigen pulsation. Positively, the passive guidance forces are enough to produce the main force component. But, additional damping actuators are necessary to provide the required damping to control the dynamic oscillations due to track profile, track dynamics and aerodynamics.

Consequently, the total guidance force has two components: a) the passive guidance force produced by the reluctance effect of the long stator reacting with the magnetic way; b) the active damping force of the additional actuators.

The *active damping system* has the advantage, on one hand, to limit the amplitude of the transverse motion generated by dynamic perturbations close to the eigen frequencies and, on the other hand, to offer a much higher quality of comfort It has the disadvantage to add equipments on board of the vehicle. The authors present the active damping actuator design. The design is fully optimized, by the use of a software[(7)] specifically dedicated to optimization process, and then confirmed with FEM 3D analysis.

The dynamics of the vehicle in motion is modeled using Simulink[8].

Finally, the spatial integration of these active damping actuators is presented, considering the other electromechanical components such as: the fixed long stator of the linear motor, the motor magnetic way (motor poles and levitation windings), on board of the vehicle and the main body of the vehicle.

2 DAMPING ACTUATOR SPECIFICATIONS

All specifications are given in references[3,4,5,6]. Two cases are considered for the vehicle guidance, as shown in Figure 1.

Specification 1 - passenger comfort: for an acceleration $a_{comfort}$ of 0.8 [m/s^2], a vehicle mass $m_{vehicle}$ of 80 [tons] and a non-total compensation of the acceleration, the guidance force is equal to:

$$F_{guidance}=m_{vehicle}\cdot a_{comfort}=64000 \quad [N] \quad (1)$$

Specification 2 - vehicle at stalls: when the vehicle stalls, in a curve of 9.66 [°] maximum inclination, the force becomes:

$$F_{guidance}=m_{vehicle}\cdot g\cdot \sin(\alpha)=134240 \quad [N] \quad (2)$$

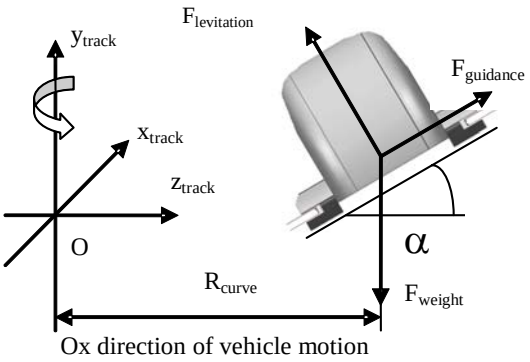

Figure 1. Vehicle in a curve: inclination α, radius R_{curve}

3 PASSIVE GUIDANCE FORCES

The passive guidance forces were determined by carrying out 2D and 3D FEM simulations[5]. Figure 2 gives the spatial distribution of the flux lines around the air-gap in a transverse plane. The passive guidance forces were determined in a steady state (constant vehicle speed and constant transverse eccentricity). Figure 3 represents the passive guidance forces corresponding to this case.

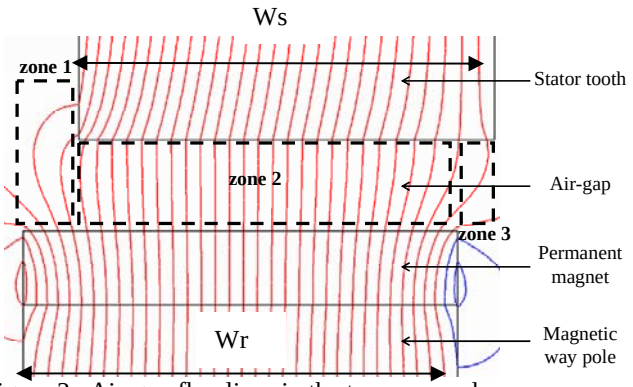

Figure 2. Air-gap flux lines in the transverse plane
Wr=94 mm; Ws=90 mm; Air gap=20 mm;
Lateral eccentricity Zz=10 [mm]

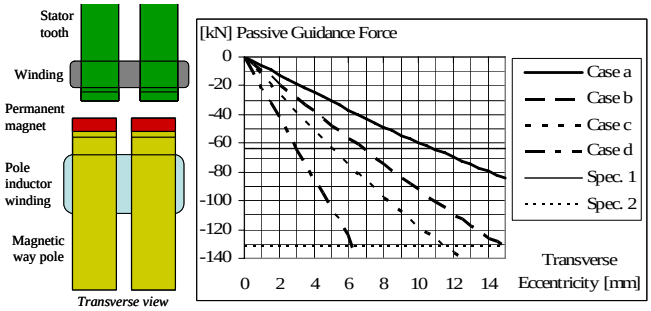

Figure 3. 3D FEM - Passive guidance force versus transverse offset (cases b, d, see fig. 3, on the left).

Single magnetic way: a: Wr=112 mm; Ws=90 mm; Air gap =20 mm;
c: Wr=112 mm; Ws=90 mm; Air gap =10 mm;

Two magnetic ways: b: Wr=56 mm; Ws=45 mm; Air gap =20 mm;
d: Wr=56 mm; Ws=45 mm; Air gap =10 mm.

For a single magnetic way of the linear synchronous motor, corresponding to case a) of Figure 3, the gradient of the passive guidance force, for the complete vehicle, is equal to $k_z=5.82\cdot10^6$ [N/m], which value is considered for the design of the active damping actuators. Furthermore, the force appears to be linear for the considered transverse eccentricities.

4 MECHANICAL SYSTEM

In order to determine the main dimensions of the damping function, the vehicle, the right track (r) and the left track (l) are simplified as shown in Figure 4. For the dynamic behavior, the following assumptions are defined:

- the vehicle is considered as rigid in the directions x_s, x_w (propulsion) and y_s, y_w (levitation);
- the vehicle speed $v_{vehicle}$ is constant;
- the motor air gap is constant: $\delta=20\pm2$ [mm].

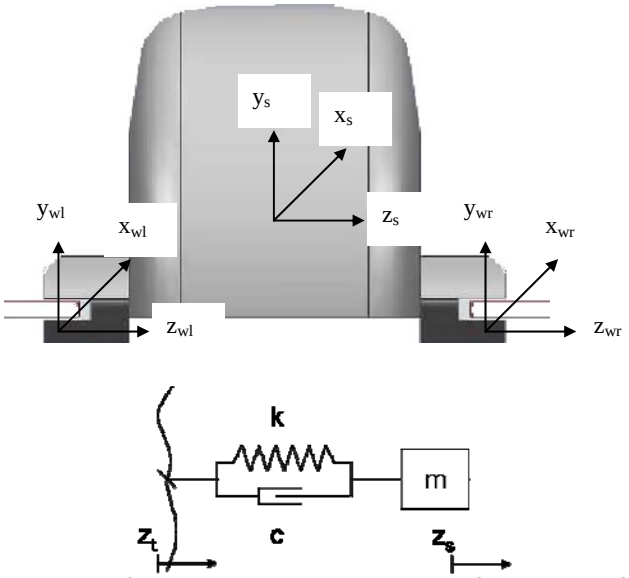

Figure 4. Referential and mechanical system for the simplified 1D model. Zt coordinate of the real track profile.

The equation of motion for this model is:

$$m_{vehicle} \cdot \ddot{z}_s = -k_z \cdot (z_s - z_t) - c \cdot (\dot{z}_s - \dot{z}_t) \qquad (3)$$

The elementary oscillator associated to this equation is well known and described, for example in Reference[9]. The real track profile is approximated by a sinusoidal function of periodicity D_{track} with a maximal deviation d versus the ideal track, as presented in Figure 5.

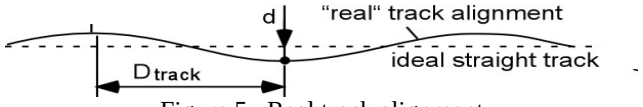

Figure 5. Real track alignment

Defining the system referential of Figure 4 and the denomination used in Figure 5, the real track (index t) has a profile defined in Equation 4.

$$\left.\begin{aligned} x_{tr} &= x_{tl} = v_{vehicle} \cdot t \\ y_{tr} &= y_{tl} = Yt = constant \\ \omega_{track} &= \frac{\pi}{D_{track}} \cdot v_{vehicle} \\ z_{tr} &= d \cdot \sin(\omega_{track} \cdot t) \\ z_{tl} &= d \cdot \sin(\omega_{track} \cdot t + \beta_0) \end{aligned}\right\} \qquad (4)$$

$$\left.\begin{aligned} \dot{x}_{tr} &= \dot{x}_{tl} = v_{vehicle} \\ \dot{y}_{tr} &= \dot{y}_{tl} = 0 \\ \dot{z}_{tr} &= d \cdot \omega_{track} \cdot \cos(\omega_{track} \cdot t) \\ \dot{z}_{tl} &= d \cdot \omega_{track} \cdot \cos(\omega_{track} \cdot t + \beta_0) \end{aligned}\right\} \qquad (5)$$

5 ACTIVE DAMPING ACTUATORS

5.1 Design Criteria

5.1.1 Ideal Viscous Damping

A first approach to determine the additional active electromechanical system is based on the knowledge of the ideal viscous damping coefficient[6] c. Considering the following relations[7], the coefficient k_z is the gradient of the lateral passive guidance force (equivalent to a spring constant) and $\dot{z}_{max}$ is the maximum lateral oscillating speed. The maximum oscillating speed is determined for the eigen frequency due to the track profile, as a maximal value based on experience and simulations[11]. Table 1 gives the corresponding characteristics.

Table 1 Track characteristics leading to a eigen frequency

D_{track}	d	$v_{vehicle}$	$\omega_{trac}k$	$\dot{z}_{max}$
[m]	[mm]	[m/s]	[1/s]	[m/s]
50.4	3.0	139	8.66	0.026

$$c = 2 \cdot \sqrt{m_{vehicle} \cdot k_z} = 1.364 \cdot 10^6 \quad [Ns/m] \qquad (6)$$

$$F_{damping} = c \cdot \dot{z}_{max} = 35477 \quad [N] \qquad (7)$$

$$F_{actuator} = \frac{F_{damping}}{N_{actuator}} = \frac{35477}{4 \cdot 6} = 1478 \quad [N] \qquad (8)$$

Each vehicle side (left and right) will have twenty four inductors.

The force $F_{damping}$ is about 55% of the nominal guidance force of 64 [kN]. The vehicle has six cells: four cells for the passengers, a nose cell and a tail cell. Each of these six cells will have four active damping actuators. The corresponding force of one inductor of the active electromechanical system is then about -1.5 [kN]. This low force value allows considering positively the problem of the heat dissipation of these inductors, in the partial vacuum (<10 kPa) of the tunnels.

5.1.2 Power Losses

The active actuators generate two types of power losses: the power losses related to the aerodynamic drag force generated by the front surface of the actuator, facing the air flow and the copper losses of the winding. The damping actuator design is achieved in order to minimize these losses in regards with the mass of the actuator.

5.1.3 Convection Coefficients

The heat dissipation is mainly considered as convection due to the air flow surrounding the

actuators. The convection coefficients are determined based on 3D air flow FEM studies[3)] of the vehicle in the tunnel. Figures 6, 7 and Table 2 show the different results obtained from these simulations.

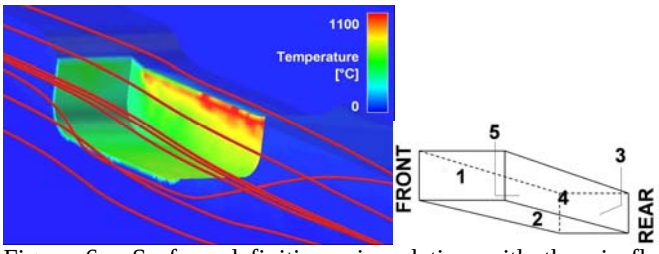

Figure 6. Surface definitions, in relation with the air flow distribution

Table 2 Convection coefficients versus the vehicle speed

	100 [km/h]	200 [km/h]	300 [km/h]	400 [km/h]
	Coefficient	Coefficient	Coefficient	Coefficient
Surface	[W/(m^{2}K)]	[W/(m^{2}K)]	[W/(m^{2}K)]	[W/(m^{2}K)]
1	23.3	40.6	56.2	70.7
2	17.3	30.2	41.7	52.5
3	9.3	16.2	22.4	28.2
4	14.1	24.5	33.8	42.6
5	11.7	20.4	28.3	35.6

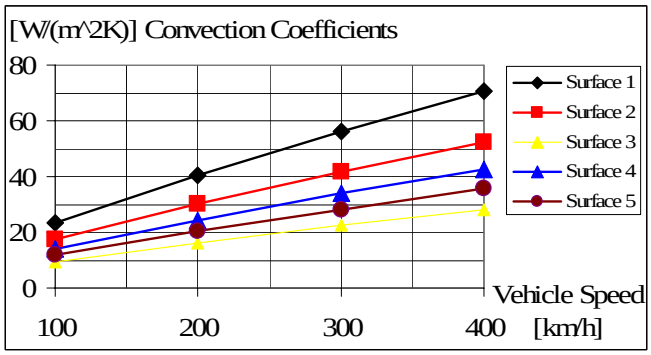

Figure 7. Convection coefficients versus vehicle speed.

5.1.4 Actuator Design Optimization

The optimization criterion of the actuator is chosen in such way to minimize the following objective function:

$$\text{Function} = \min\left[\left(P_{cu} + P_{aero}\right)\cdot m_{inductor}\right] \quad [\text{W}\cdot\text{kg}] \qquad (9)$$

Where P_{cu} are the copper losses and P_{aero} are the aerodynamic drag force losses and $m_{inductor}$ the mass of the inductor on board of the vehicle.

5.2 Actuator Design

The actuator is a simple electromagnetic inductor working as a reluctant system, as presented in Figure 8. The inductor with its winding is on board of the vehicle, the corresponding reactive laminated rail is fixed with the track. An air gap of 20 [mm] is imposed. The optimization process of the design is based on Pro@Design[(7)] software. The optimization process requests the knowledge of all equations related to the design: some are used to express the objective function and the others to define the constraints. Here, only the key equations are presented out of a total of 65 independent equations.

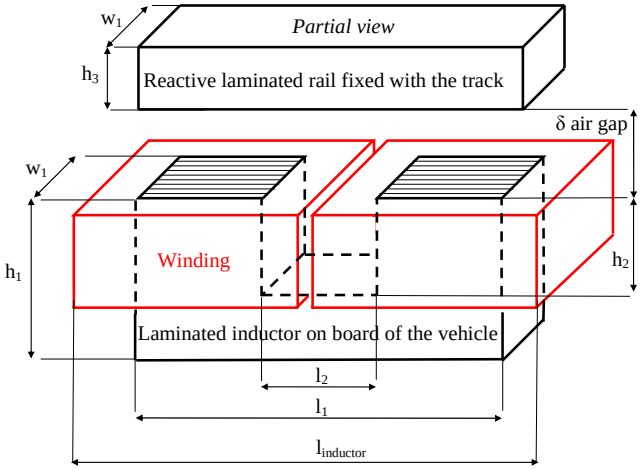

Figure 8. Active damping actuator

5.2.1 Magnetic Equations

Based on the geometry, as shown in Figure 8, a magnetic lumped scheme is defined in Figure 9. The key equations are presented in the following chapters.

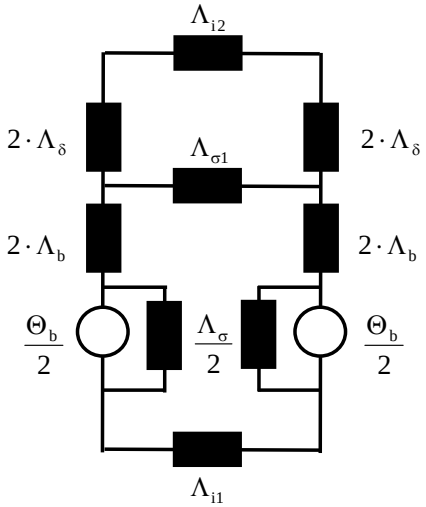

Figure 9. Simplified magnetic lumped scheme

5.2.2 Surfaces

The main surfaces of the inductor are defined as follows:

The air gap surface:

$$A_{\delta} = \frac{l_1 - l_2}{2}\cdot w_1 \qquad [\text{m}^2] \qquad (10)$$

Iron surface of the tooth inductor:

$$A_b = k_{f1}\cdot A_{\delta} \qquad [\text{m}^2] \qquad (11)$$

Iron surfaces of the inductor yoke and the reactive rail:

$$A_{i1} = k_{f1} \cdot (h_1 - h_2) \cdot w_1 \quad [m^2] \quad (12)$$

$$A_{i2} = k_{f2} \cdot h_3 \cdot w_1 \quad [m^2] \quad (13)$$

Copper surface in the slot of the inductor:

$$A_{cu} = k_{cu} \cdot h_2 \cdot l_2 \quad [m^2] \quad (14)$$

Convection surfaces (1, 2, 3, 4, 5), as shown in Figure 6:

$$A_1 = w_{inductor} \cdot \left(h_2 + \frac{l_2}{2}\right) + (h_1 - h_2) \cdot w_1 \quad [m^2] \quad (15)$$

$$A_2 = w_1 \cdot l_1 \quad [m^2] \quad (16)$$

$$A_3 = A_1 \quad [m^2] \quad (17)$$

$$A_4 = l_{inductor} \cdot \left(h_2 + \frac{l_2}{2}\right) + l_1 \cdot (h_1 - h_2) \quad [m^2] \quad (18)$$

$$A_5 = A_4 \quad [m^2] \quad (19)$$

5.2.3 Permeances

The permeances of the scheme are expressed as follows. The air gap surface permeance:

$$\Lambda_\delta = \mu_0 \cdot \frac{A_\delta}{2 \cdot \delta} \quad [H] \quad (20)$$

The permeance of the tooth inductor:

$$\Lambda_b = \mu_0 \cdot \mu_{i1} \cdot \frac{A_b}{2 \cdot l_b} \quad [H] \quad (21)$$

The inductor yoke and the reactive rail permeances:

$$\Lambda_{i1} = \mu_0 \cdot \mu_{i1} \cdot \frac{A_{i1}}{l_{i1}} \quad [H] \quad (22)$$

$$\Lambda_{i2} = \mu_0 \cdot \mu_{i2} \cdot \frac{A_{i2}}{l_{i1}} \quad [H] \quad (23)$$

$$\Lambda_1 = \frac{\Lambda_{i2} \cdot \Lambda_\delta}{\Lambda_{i2} + \Lambda_\delta} + \Lambda_{\sigma 1} \quad [H] \quad (24)$$

And finally, the equivalent scheme permeance:

$$\Lambda_{bb} = (1 + k_\sigma) \cdot \frac{\Lambda_b \cdot \Lambda_{i1} \cdot \Lambda_1}{\Lambda_{i1} \cdot \Lambda_1 + \Lambda_b \cdot \Lambda_1 + \Lambda_b \cdot \Lambda_{i1}} \quad [H] \quad (25)$$

5.2.4 Magnetic Potential, Flux and Flux Densities

The magnetic potential, the flux and the flux densities are expressed, taking into account the magnetic characteristics of the chosen lamination.

The total magnetic potential:

$$\Theta_b = J_{cu} \cdot A_{cu} \quad [A] \quad (26)$$

The total flux:

$$\Phi_{tot} = \Lambda_{bb} \cdot \Theta_b \quad [Vs] \quad (27)$$

$$\Phi = (\Lambda_{bb} - \Lambda_\sigma) \cdot \Theta_b \quad [Vs] \quad (28)$$

The air gap flux density:

$$B_\delta = \frac{\Phi}{A_\delta} \cdot \left(1 - \frac{\Lambda_{\sigma 1}}{\Lambda_1}\right) \quad [T] \quad (29)$$

The flux density of the tooth inductor:

$$B_b = \frac{\Phi}{A_b} \quad [T] \quad (30)$$

$B_b = B_1(H_b)$, B(H) curve of the inductor lamination

[T] (31)

The inductor yoke and reactive rail flux densities:

$$B_{i1} = \frac{\Phi}{A_{i1}} \quad [T] \quad (32)$$

$B_{i1} = B_1(H_{i1})$, B(H) curve of the inductor lamination

$$B_{i2} = B_\delta \quad [T] \quad (33)$$

$B_{i2} = B_2(H_{i2})$, B(H) curve of the inductor lamination

[T] (34)

5.2.5 Copper Losses – Heat Dissipation

The copper losses considering the permanent temperature $T_{permanent}$ and the coefficient of the duty cycle of the inductor k_{duty} are expressed as follows:

$$\rho_{cu} = 17e^{-9} \cdot (1 + 0.004 \cdot (T_{permanent} - 15)) \quad [Ohm \cdot m] \quad (35)$$

$$P_{cu} = \rho_{cu} \cdot J_{cu}^2 \cdot V_{cu} \quad [W] \quad (36)$$

$$P_{ave} = k_{duty} \cdot P_{cu} \quad [W] \quad (37)$$

$$\left.\begin{aligned} \Delta T &= \frac{P_{ave}}{\alpha_1 \cdot A_1 + \alpha_2 \cdot A_2 + \alpha_3 \cdot A_3 + \alpha_4 \cdot A_4 + \alpha_5 \cdot A_5} \\ T_{permanent_{max}} &\geq T_{ambiant} + \Delta T \end{aligned}\right\} \quad [K] \quad (38)$$

The coefficients $\alpha_1, \alpha_2, \alpha_3, \alpha_4, \alpha_5$ are the convection coefficients determined in Chapter 5.1.3 and the surfaces A_1, A_2, A_3, A_4, A_5 the outside surfaces of the inductor as described in Figure 6. The maximum temperature is defined by the chosen insulation class of the winding.

5.2.6 Aerodynamic Drag Power

The inductor frontal surface $A_{frontal}$ creates an aerodynamic drag force, leading to power losses P_{aero} to be furnished by the motor propulsion. The aerodynamic power losses are expressed as:

$$v_{air} = 1.2 \cdot v_{vehicle} \quad [m/s] \quad (39)$$

$$P_{aero} = C_x \cdot \gamma_{air} \cdot A_{frontal} \cdot \frac{v_{air}^3}{2} \quad [W] \quad (40)$$

$$C_x = 0.85 \quad [-] \quad (41)$$

where γ_{air} is the mass per volume unit of air.

5.2.7 Guidance Force

The force produces by the actuator is then defined as:

$$F_\delta = 2 \cdot \frac{d\Lambda_{bb}}{d\delta} \cdot \Theta_b^2 \qquad [N] \qquad (42)$$

$$F_\delta = k_F \cdot \frac{i_b^2}{\delta^2} \qquad [N] \qquad (43)$$

Around a working point (i_b, δ) and for small variations of the current or the air gap, the coefficient k_f does not change (local linearization).

5.2.8 Results and Design Choice

The actuator design optimization gives a set of designs since the vehicle speed is a variable parameter. Table 3 and Figure 10 show the different obtained optimum designs. All designs deliver 1.5 [kN] force for a 20 [A] nominal current.

Table 3a Dimensions issued from the optimization

Speed	l_1	l_2	W_1	h_1	h_2	Length	Width
[km/h]	[m]	[m]	[m]	[m]	[m]	[m]	[m]
100	0.338	0.100	0.110	0.184	0.128	0.324	0.161
200	0.341	0.108	0.107	0.112	0.064	0.358	0.154
300	0.373	0.132	0.116	0.079	0.036	0.479	0.231
400	0.389	0.157	0.120	0.064	0.024	0.528	0.266

Table 3b Characteristics issued from the optimization

Speed	Mass	P_{ave}	P_{aero}	N_b	i_b	U_{dc}	k_f
[km/h]	[kg]	[W]	[W]	[-]	[A]	[V]	[Nm^2/A^2]
100	85	223	62.1	304	20	20.91	-1.50E-03
200	49	477	282.7	311	20	44.76	-1.50E-03
300	40	676	709.8	294	20	63.39	-1.50E-03
400	35	911	1383	295	20	85.38	-1.50E-03

Table 3c Characteristics issued from the optimization

Speed	Llb	Rrb	Time constant
[km/h]	[H]	[Ohm]	[s]
100	0.156	0.697	0.224
200	0.0881	1.492	0.059
300	0.0869	2.113	0.041
400	0.0839	2.846	0.029

For a force of 1.5 [kN], at low speed, the heat dissipation leads to an increase of the surfaces in order to compensate the decrease of the convection coefficients. Consequently, the design corresponding to the minimum mass of the actuator, occurring at a 400 [km/h] cannot be considered for a final choice, since it will lead to non authorized heating for low speeds. A compromise has to be done between the mass and the heating at low speed. The design corresponding to a speed of 200 [km/h] is chosen.

5.2.9 FEM 3D Simulations

Finite element method is used to confirm the previous design choice. Figures 10 to 12 present the main results where the effect of the flux fringes in the air gap increase favorably the force. Figure 11 shows that a leakage permeance should appear in parallel with the permeance Λ_{i1} in the scheme.

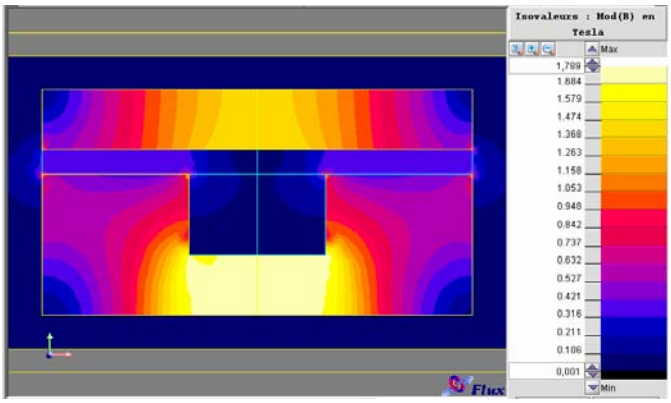

Figure 10. FEM 3D simulations – Medium inductor plane – Flux densities for i_b=20 [A], δ=20 [mm]

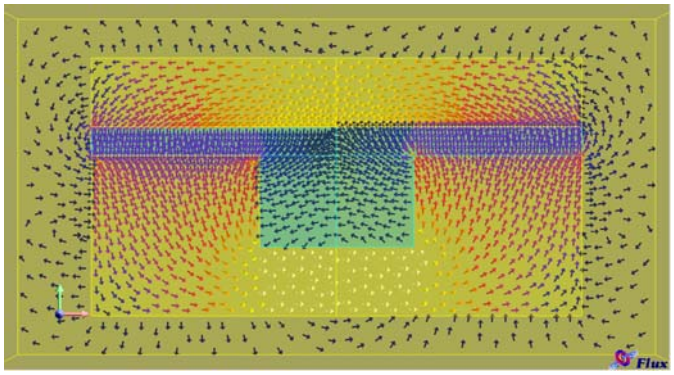

Figure 11. FEM 3D simulations – Medium inductor plane – Flux density vectors for i_b=20 [A], δ=20 [mm]

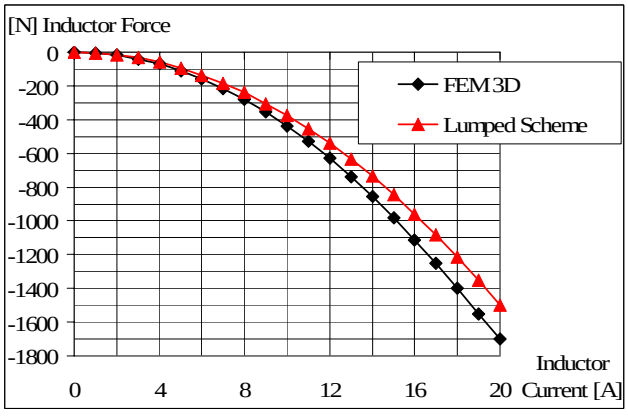

Figure 12. Inductor force – FEM 3D simulations and lumped scheme simulation, for δ=20 [mm]

6 DYNAMICS OF THE SYSTEM

6.1 Preliminary Considerations

Swissmetro system is characterized by a diameter tunnel of 5.70 [m], the wall stiffness of which is considerably high. This characteristic is highly useful

to control the dynamics of the vehicle in interaction with the guide way. The reactive rail can be fastened close to the tunnel wall and the guide way elements length can be small in order to achieve a highly stiff guide way with high eigen frequencies. The topology of the vehicle and tunnel allows also having the electromechanical actuators located as close as possible to the tunnel wall: the force lines are therefore short. All these characteristics are leading to a highly rigid and stable guide way. This guide way can be accurately fastened by robots leading to a high precision in its geometry. For the case of Swissmetro, it is therefore reasonable to consider the guide way as rigid. Moreover, the choice of a 20 [mm] air gap makes it possible to simplify the vehicle architecture and to work with only one level of suspension.

6.2 Validation of Actuator Design

The validation of the above-presented actuator design is done through the use of a dynamic model for one complete vehicle cell.

6.2.1 Vehicle Model

As indicated in Chapter 5.1.1, the vehicle is made of six cells. Swissmetro being entirely underground, it is possible to design lines with high curve radius of 5000 [m] minimum value. This reduces the deflection between two adjacent cells. A flexible coupling between two cells has been developed, this coupling allows to have a high stiffness in the longitudinal direction (Ox) and flexibility transversally (Oy and Oz). Therefore, the cells are independent to each other, regarding transverse forces and movement.

The cell can be modeled as shown on Figure 13 using the following equations:

$$m_{cell} \cdot \ddot{z}_s = -k_{zm} \cdot (z_{sm} - z_{tm}) + \sum F_{DIn} \quad (44)$$

$$m_{cell} \cdot \ddot{\theta} = -k_{zm} \cdot (z_{sm} - z_{tm}) \cdot x_{MWm} + \sum F_{DIn} \cdot x_{DIm} \quad (45)$$

Where:

- The mass of the passenger cell m_{cell} is 12.5 [tons];
- k_{zm} is the contribution of the magnetic way of index m to the gradient of the passive guidance force. We have the relation $\Sigma\, k_{zm}=k_z$. The model is made of 88 magnetic ways, 44 on each side of the vehicle;
- F_{DIn} is the force generated by the damping inductor of index n. The amplitude of this force is calculated using equation (43);
- The inertia of the cell I_{cell} is 175000 [kg m^2];
- θ is the angle of yaw of the cell in [rad];
- x_{MWm} is the position of the magnetic way of index n along the x axis in the referential of the gravity center;
- x_{DIn} is the position of the damping inductor of index n along the x axis in the referential of the gravity center.

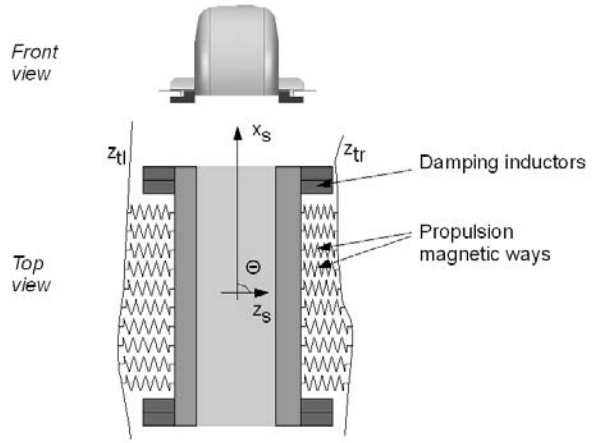

Figure 13. Mechanical system for one passenger cell. Theta (θ) represents the yaw angle.

The system presented in Figure 13 has been modeled in Simulink. The model can accept two different track profiles (z_{tl}, left, and z_{tr}, right). The simulations were undertaken at a speed of the vehicle of 139 [m/s].

6.2.2 Simulation Results

The dynamic response of this model in opened-loop (F_{di}=0) is presented in Figure 14. The shape of both guide ways (left and right) is the same and corresponds to the case of Table 1 (d=3 [mm]).

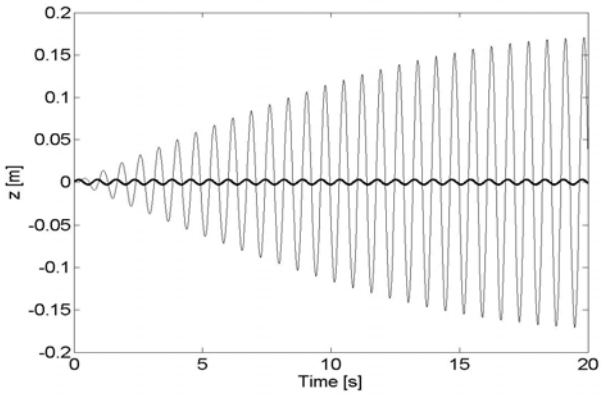

Figure 14. Opened-loop response for the passenger-cell model undertaking a sine track perturbation (z_s grey line, z_t dark line, β_0=0).

It can be seen that the energy accumulation at eigen-frequency is leading to an unstable behavior. The damping action of the inductors is required to stabilize the vehicle lateral movement. The controller of the damping inductors is based on a simple proportional feedback control based on the velocity of lateral motion. The inductor itself is modeled on the basis of Equation (43).

The closed-loop response of the vehicle with the same guide way perturbation is presented in Figure 15.

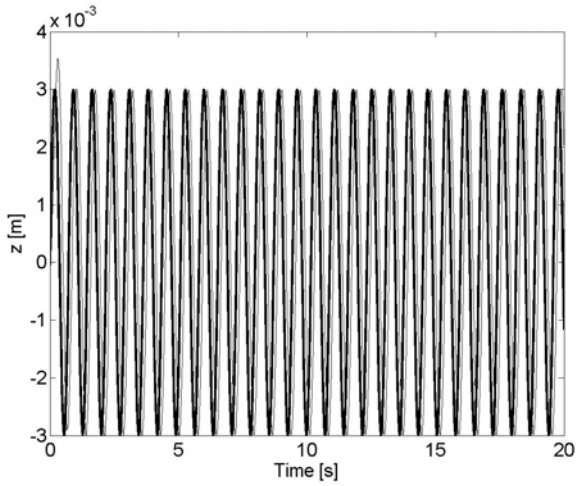

Figure 15. Closed-loop response for the passenger-cell model undertaking a sine track perturbation (z_s grey line, z_t dark line, β_0=0).

It can be seen that the damping is very efficient and that the vehicle follows the guide way with a small phase difference. Figure 16 shows the current in one of the damping inductor.

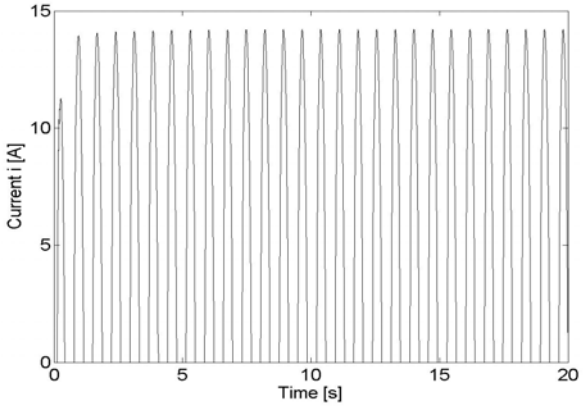

Figure 16. Current in the damping inductors corresponding to the case presented in Fig. 15.

The currents are 30% below the nominal current of 20 [A]. The design is therefore safe and additional damping force is available for additional contribution to lateral motion (such as aerodynamic instabilities, mechanical structures deformation).

Finally, the dynamic response of the vehicle model to steps is presented in Figure 17. One step of 3 [mm] in height occurs on the left guideway after 2 seconds. An additional step of 3 [mm] in height occurs at 7 seconds on the right guide way. Both steps are in the same direction. Figure 17 shows the opened-loop response and Figure 18 and 19 correspond to the closed-loop responses.

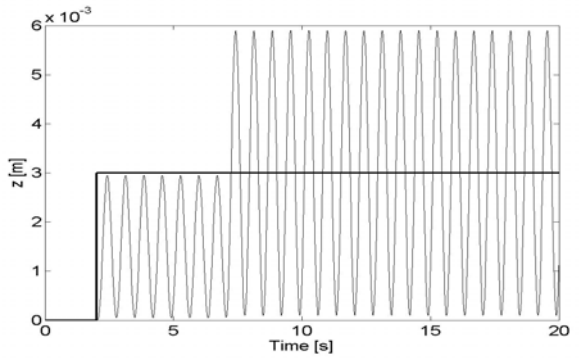

Figure 17. Opened-loop response to two perturbation steps of the track profile (z_s grey line, z_t dark line).

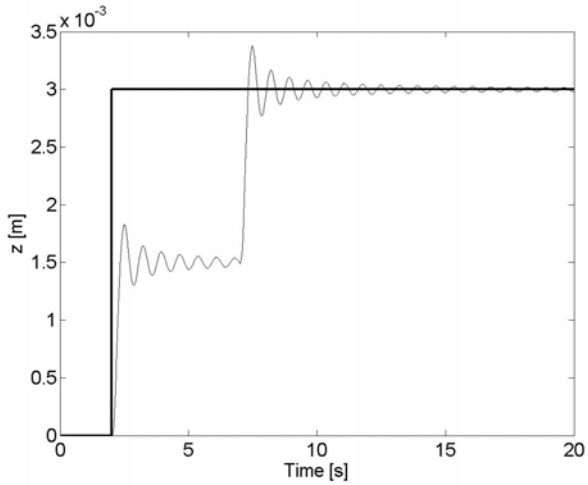

Figure 18. Closed-loop response to two perturbation steps of the track profile (z_s grey line, z_t dark line).

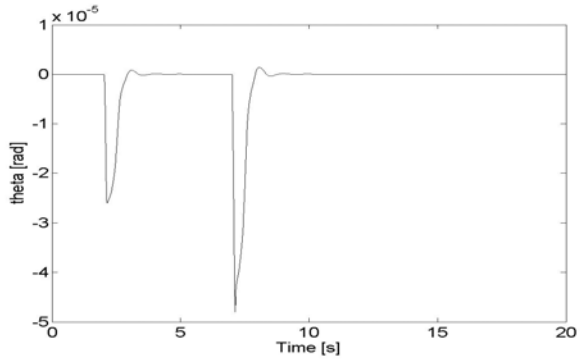

Figure 19. Closed-loop response to two perturbation steps, yaw angle (theta).

The analysis of the different Figures shows that the expected behavior is reached and that the vehicle lateral motion can be efficiently damped by the damping inductors.

6.2.3 Case of Low Sine Wave of the Track Profile

The following example is characterized by a low sine frequency (0.5 [rad/s], amplitude of 5 [mm]) on track left and a step of -5 [mm] at 7 [s] on right track. The

results for opened-loop and closed-loop are presented in Figure 19.

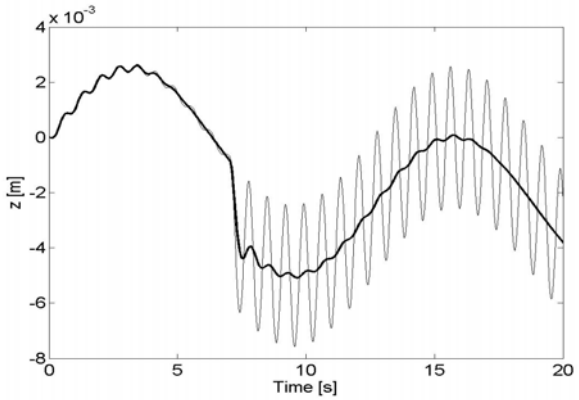

Figure 19. Lateral motion of the vehicle – grey line: opened-loop response to 1 step and 1 sine perturbation; dark line: closed-loop.

The analysis of the acceleration shows the improvement provided by the damping actuators on the comfort of the passengers.

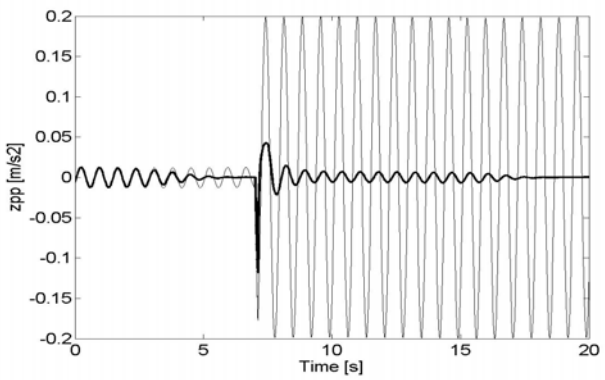

Figure 20. Acceleration in the passenger cell - light line: opened-loop response to 1 step and 1 sine perturbation, thick line: closed-loop.

Figure 21 shows the variation of the yaw angle in the same conditions.

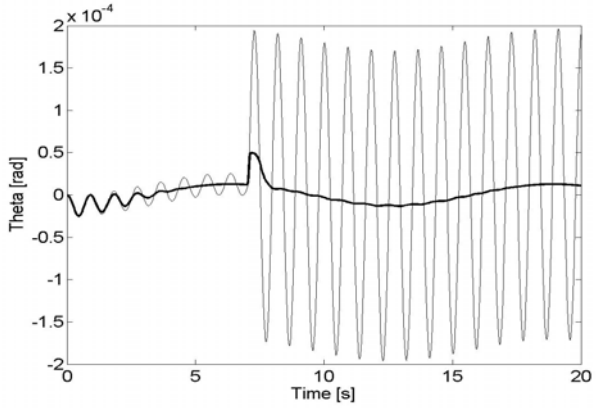

Figure 21. Yaw angle theta of the passenger cell - grey line: opened-loop response to 1 step and 1 sine perturbation; dark line: closed-loop.

7 SPATIAL INTEGRATION

Considering the top view on Figure 13, the eight damping inductors needs to be placed at the extremities of the cell, on each side. This location allows maximizing the efficiency of yaw angle control.

The motor magnetic way (excitation poles and levitation coils) is located along the vehicle, symmetrically to the center of gravity.

8 CONCLUSIONS

The design, the optimization and the validation of damping inductors having the function to stabilize the lateral motions of the vehicle has been done successfully.

The role of these inductors is to complement the passive centering force generated by the motor magnetic way, which is characterized by a very low damping[6]. In particular, these inductors need to provide an active damping force to avoid instabilities at eigen-frequencies. In order to stabilize the lateral motion, eight damping inductors acting on each of the 6 cells of the vehicle have been designed and integrated to the structure concept.

The behavior of one cell of the vehicle (simplified rigid model with 2 DOF) has been modeled and simulations allowed verifying the design.

The whole design process has been validated. In particular, the use of optimization software allows to handle the complexity of the design choices and to efficiently support decisions in design phase.

With the damping inductors installed on each cell of the vehicle, the lateral dynamics of the vehicle can be controlled.

The paper showed that a standard proportional regulation on lateral velocity is sufficient to achieve already good riding performances. Additional work is necessary in order to optimize the control strategy of these new inductors.

9 LIST OF SYMBOLS

D	track: half period of alignment	[m]
Fz	force (z component)	[N]
a	acceleration	[m/s^2]
d	track deflection	[m]
g	earth acceleration	[m/s^2]
k	force constant	[N/m]
kz	force constant (guidance force)	[Ns^2/m^2]
m	mass	[kg]
t	time	[s]

v	vehicle speed	[m/s]
x	coordinate (motion direction)	[m]
y	coordinate (vertical direction)	[m]
z	coordinate (lateral direction)	[m]
β_0	shift between left tand right track profiles	[m]
δ	air gap	[m]
ω	pulsation	[1/s]

Indexes

l	left
r	right
t	track
s	stator
w	magnetic way

10 REFERENCES

1. A. Cassat, M. Jufer, "MAGLEV Projects Technology Aspects and Choices", IEEE Transactions on Applied Superconductivity, Vol. 12, Issue 1, March 2002, pp: 915-925.
2. A. Cassat, C. Espanet, "SWISSMETRO: Combined Propulsion with Levitation and Guidance", MAGLEV 2004, October 26-28, 2004, Shanghai, China, Proceedings, pp 747-758, vol. II.
3. A. Cassat, C. Espanet, V. Bourquin, P. Hagmann, M. Jufer, "SWISSMETRO - Polarized Linear Motor Combined With Levitation Actuators", LDIA 2005, September 25-28, 2005, pp 247-250, Awaji Yumebutai, Hyogo, Japan and also
4. Reference [3] is also in IEEJ Trans. IA, VOL 126, No. 10, pp 1286-1292, 2006.
5. A. Cassat, C. Espanet, V. Bourquin, M. Jufer, "Passive Guidance Forces of Polarized Linear Motors Combined with Levitation Actuators Working in Partial Vacuum – Application to Swissmetro", MAGLEV 2006, September 13-15, 2006, Dresden, Germany, Vol. I, pp 351-362.
6. A. Cassat, C. Espanet, V. Bourquin, Y. Perriard, "Dynamic of Passive Guidance Forces of Polarized Linear Motors - Application to Swissmetro", LDIA 2007, September 16-19, 2007, Lille, France, Proceedings, CD-ROM.
7. Pro@Design, http://designprocessing.free.fr/
8. Matlab/Simulink, http://www.mathworks.com.
9. M. Del Pedro, P. Pahud: “Mécanique vibratoire: systèmes discrets linéaires”, Presses Polytechniques Romandes, Lausanne, 1989.
10. M. Zayadine, “Etude de réglage en position de la sustentation magnétique par attraction”, Thèse numéro 1508, Ecole Polytechnique Fédérale de Lausanne, Lausanne, 1996.
11. H. Dupraz, W. Coosemans, F. Ossart, V. Bourquin : “Projet HISTAR : Alignement par écartométrie biaxiale d’une maquette de train à très grande vitesse”, Revue XYZ, no 83, p. 65-69, 2000.